Journal of Zhejiang University-SCIENCE A in press
www.jzus.zju.edu.cn; www.springer.com/journal/11582
E-mail: jzus_a@zju.edu.cn

Research Article
https://doi.org/10.1631/jzus.A2600314

Flutter characteristics of a two-dimensional prepositive elliptical wing–main wing combined configuration

Congyu ZHAO[1,2], Baigang MI[1✉], Xuan BAI[1,2]

[1]*Northwestern Polytechnical University, School of Aeronautics, Xi'an, 710072, China*
[2]*National Key Laboratory of Aircraft Configuration Design, Xi'an, 710072, China*

Abstract: Flutter is a complex dynamic aeroelastic problem that poses a significant threat to flight safety, making its mitigation a critical focus of aeronautical research. This study proposes a two-dimensional prepositive elliptical wing–main wing combined configuration and investigates its influence on flutter characteristics. Based on structural dynamics, a reduced-order aeroelastic model of the two-dimensional combined configuration is established. The critical flutter velocities of configurations with and without the prepositive elliptical wing are computed using the eigenvalue method. The results from a representative case show that the configuration yields a critical flutter speed enhancement of up to 43.59%. Through a parametric design space exploration, a range of effective design parameters is identified: for chordwise placement within 0.04c (where c is the main wing chord) directly in front of the main wing, a pre-wing with a long axis of 0.02c, short axis of 0.005c, and aspect ratio of 4 is recommended. For distances beyond 0.04c, a diagonal arrangement above and ahead of the main wing is more effective, with a recommended long axis of 0.01c, a short axis of 0.005c, and an aspect ratio of 2.

Key words: Aeroelasticity; Eigenvalue method; Passive flow control; Numerical simulation

1 Introduction

Flutter is a self-excited aeroelastic instability caused by the coupling among aerodynamic, elastic, and inertial forces. When the aerodynamic energy input during structural oscillation cannot be dissipated by structural damping, the vibration amplitude may increase rapidly and eventually threaten flight safety (Guo et al., 2025). With the increasing demand for lightweight, flexible, and high-performance aircraft, flutter prediction and flutter-boundary improvement remain essential issues in aeroelastic design. Previous studies have therefore attempted to delay flutter onset by modifying structural parameters, aerodynamic layouts, or control strategies. These studies show that flutter is not only a structural-dynamic problem but also a configuration-dependent aerodynamic problem in which the phase relationship between aerodynamic forces and structural motion plays a decisive role.

One important route for improving flutter characteristics is wing design. Aeroelastic tailoring modifies the stiffness distribution and coupling behavior of a wing by optimizing composite-material layups, fiber orientations, and structural layouts. Through favorable bend-twist coupling and directional stiffness design, aeroelastic tailoring can increase flutter speed while maintaining aerodynamic efficiency and reducing structural weight (Najmi et al., 2024). Similar design-oriented studies indicate that the flutter boundary is strongly affected by the stiffness distribution, mass distribution, elastic-axis location, and aerodynamic configuration. These results suggest that configuration-level design can provide a useful way to improve aeroelastic stability.

Accurate prediction of the flutter boundary requires an appropriate aeroelastic analysis method. Traditional flutter analysis is generally based on the coupling between structural dynamic equations and unsteady aerodynamic models. The critical flutter speed is then obtained by solving the eigenvalue

✉ Baigang MI, mibaigang@163.com
Congyu ZHAO, https://orcid.org/0009-0006-0253-9319

Received May 14, 2026; Revision accepted June 29, 2026; Crosschecked

problem or by tracking modal damping as the flow velocity increases. Classical frequency-domain approaches, such as the p-k and k methods, are widely used because of their computational efficiency and clear modal interpretation (Borglund and Kuttenkeuler, 2002). With the development of computational resources, high-fidelity CFD and fluid-structure interaction simulations have also been increasingly applied to aeroelastic problems. Nevertheless, reduced-order models remain valuable in preliminary design and parametric studies because they allow rapid evaluation of aeroelastic trends and reveal the main influence of key parameters.

Flutter suppression methods can generally be divided into passive and active approaches. Passive methods improve the stability boundary by changing the structural parameters, mass distribution, or aerodynamic layout. More recent studies have introduced additional passive devices into wing systems to absorb aeroelastic energy. Coupled flaps, tuned mass dampers, and nonlinear energy sinks can dissipate energy near the instability boundary and improve the stability of two-dimensional wing sections (Fernandez-Escudero et al., 2023). Compared with active control, passive methods are structurally simple and reliable, but their control effect is usually fixed after design and may be sensitive to the selected configuration parameters.

Active flutter suppression has also been extensively investigated. Classical active-control strategies modify the aerodynamic energy input or add modal damping through control surfaces, piezoelectric actuators, leading-edge blowing, circulation control, or feedback controllers. Early work based on aerodynamic energy concepts demonstrated that suitable control-surface motion can suppress airfoil flutter over a range of reduced frequencies (Nissim, 1971). Later studies introduced adaptive control, LQR/LQG control, robust control, output feedback, and machine-learning-based control strategies to improve stability and robustness in nonlinear aeroelastic systems (Strganac et al., 2000; Patil and Hodges, 2002; Behal et al., 2006; Theis et al., 2020; Ribeiro et al., 2025; Chen et al., 2023; Chen et al., 2012; Mu et al., 2022). Time-delay effects and morphing control surfaces have also been considered in aeroelastic control studies (Sun and Jin, 2023; Sinou, 2022; Wu et al., 2022; Ouyang et al., 2021). In addition, nonlinear hysteresis links have been studied using describing functions, polynomial hysteresis models, and unsteady vortex aerodynamic theory, providing further insight into nonlinear flutter and control-surface effectiveness (Gu and Yang, 2006; Li and Xiang, 2007; Ouyang and Gu, 2010). Although active control provides strong adaptability, it usually requires sensors, actuators, a power supply, and a control-law design, which increases system complexity and introduces additional reliability requirements.

Most flutter suppression methods modify existing aircraft components to regulate aerodynamic energy and modal coupling, which may also alter the original aerodynamic characteristics. The prepositive elliptical wing–main wing combined configuration (abbreviated as pre-main wing) provides a flow-control-inspired alternative. Previous studies have shown that the pre-wing can disturb the wake, suppress main-wing separation, and improve aerodynamic performance without forming unnecessary drag under suitable conditions (Mi and Bai, 2022; Bai et al., 2025). However, its aeroelastic influence on the downstream main wing remains unclear.

In this study, a reduced-order aeroelastic model of the pre-main wing combined configuration is established based on structural dynamics. The critical flutter speed is calculated using the eigenvalue method, and the effects of the main design parameters are analyzed to evaluate the influence of the pre-wing on the flutter characteristics.

2 Mathematical modeling of flutter suppression in the combined configuration

2.1 Flutter suppression mechanism in the combined configuration

As a novel flutter suppression method, an elliptical wing component is installed in front of the main wing. Its purpose is to improve boundary layer flow near the main wing by using the elliptical wing to optimize flow field characteristics and to modify the energy input into the system. This results in weakening the aerodynamic force that acts on the wing system and delays flutter occurrence. Its influence is mainly associated with two mechanisms:

First, the pre-wing behaves similarly to a detached vortex-generating element, enhancing momentum exchange near the leading edge of the main wing. Unlike vortex generators, the pre-wing is installed at specific points on the wing's leading edge and forms a combined system that generates lift and reduces unnecessary drag (Bai et al., 2025). Second, the gap between the pre-wing and the main wing induces a slot-like acceleration effect, which increases the kinetic energy of the flow over the upper surface and weakens separation caused by adverse pressure gradients (Fig. 1). The pre-wing can be configured in two forms, which are stationary and vibrating (Fig. 2). Previous CFD studies showed that under high-angle-of-attack conditions, a stationary pre-wing increased the lift-to-drag ratio of an NACA0012 main wing from 4.1475 to 17.4144, corresponding to a maximum increase of approximately 319%. A small-amplitude vibrating pre-wing further increased the maximum lift-to-drag ratio by 485% (Mi and Bai, 2022). Meanwhile, within the small angle of attack range of 0-12°, the pre-wing does not exert significant adverse effects on the original lift-to-drag performance of the main wing, and the ratio even shows a slight improvement.

According to the aerodynamic energy theory of active flutter suppression, reducing the aerodynamic energy input during oscillation can delay flutter onset. The pre-wing modifies the local flow state and aerodynamic derivatives of the main wing, thereby regulating the aerodynamic stiffness and damping related to flutter without markedly impairing the baseline aerodynamic performance.

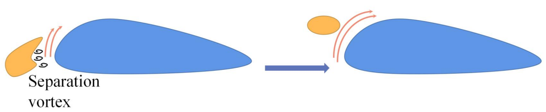

Fig. 1 Seam channel between the prepositive elliptical wing and the main wing

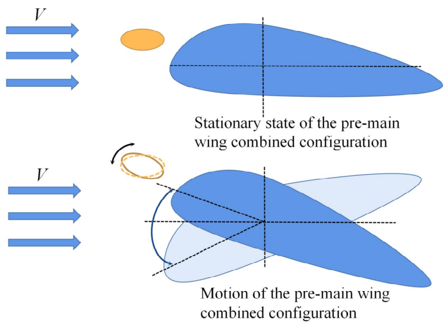

Fig. 2 Stationary and vibrating forms of the pre–main wing combined configuration

2.2 Aeroelastic modeling of the 2D combined configuration

Depending on the design parameters, the pre-wing can be placed above, directly in front of, or below the leading edge of the main wing (Fig. 3). The configuration's location and size influence flow field characteristics and wake disturbances, which in turn affect flow control at high angles of attack, alter energy input, and shift the system's flutter boundary.

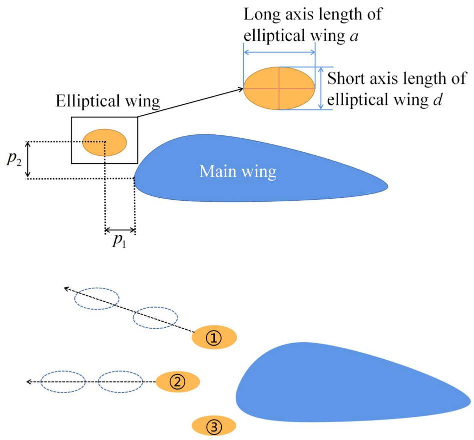

Fig. 3 Schematic diagrams of the pre–main wing system

The structural model of the pre-main wing configuration is illustrated in Fig. 4. In the present reduced-order model, the pre-wing is not used to reproduce the detailed separation process or wake evolution between the two wings. Instead, its aerodynamic influence is introduced as an equivalent disturbance to the main-wing inflow. Under the small-disturbance assumption, this influence can be linearized and represented through changes in the effective angle of attack, camber-related disturbance, and aerodynamic force distribution. Distances from the main wing's leading edge and the center of rigidity to the chord midline are denoted by l_1 and l_3, respectively. b is the distance from the leading edge of the long axis to the chord centerline.

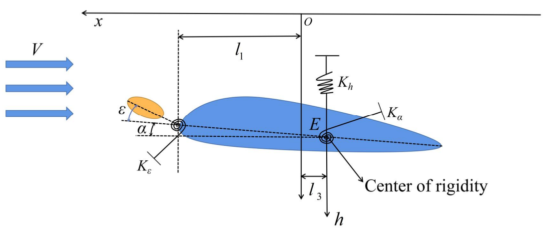

Fig. 4 Pre–main wing structural model

Accordingly, the pre-wing is modeled as an equivalent flat-plate aerodynamic element located near the leading edge of the main wing and connected through a torsional stiffness. The introduced pre-wing deflection coordinate is interpreted as a generalized aerodynamic coordinate describing the lift and pitching-moment perturbations induced by the pre-wing, rather than the prescribed motion of an active pre-wing. This treatment allows the pre-wing effect to be incorporated into the low-order aeroelastic framework through equivalent aerodynamic stiffness and damping.

Table 1 presents the design parameters for the 2D combined configuration.

Table 1 Design parameters for the 2D pre-main wing combined configuration

Type	Design parameters	Sign
Size parameters	Long axis chord length	a
	Short axis chord length	d
Position parameters	Chordwise offsets relative to the main wing	p_1
	Vertical offsets relative to the main wing	p_2
Structural parameters	Stiffness and damping of wire springs for plunging motion	K_h and C_h
	Stiffness and damping of torsion springs for pitching motion	K_α and C_α
	Stiffness of the torsion spring for pre-wing deflection motion	K_ε
Motion parameters	Plunging of the main wing(downward positive)	h
	Pitching about the center of rigidity(leading edge of the main wing upward positive)	α
	Deflection of the leading wing(leading edge deflecting upward positive)	ε

For the reduced-order aeroelastic model, the generalized coordinate vector is defined as $\mathbf{q}=[h,\alpha,\varepsilon]^{\mathrm{T}}$. Using Lagrange's equation, the structural dynamic equation and the corresponding aeroelastic equation after introducing aerodynamic terms can be written as

$$\mathbf{M}\ddot{\mathbf{q}}+\mathbf{D}\dot{\mathbf{q}}+\mathbf{K}\mathbf{q}=\mathbf{Q} \tag{1a}$$

$$\mathbf{M}\ddot{\mathbf{q}}+\tilde{\mathbf{D}}\dot{\mathbf{q}}+\tilde{\mathbf{K}}\mathbf{q}=\mathbf{0} \tag{1b}$$

where $\mathbf{M}$, $\mathbf{D}$, and $\mathbf{K}$ are the generalized mass, damping, and stiffness matrices, respectively; $\mathbf{Q}$ is the generalized aerodynamic force vector; $\tilde{\mathbf{D}}$ and $\tilde{\mathbf{K}}$ denote the equivalent damping and stiffness matrices after including aerodynamic contributions. The detailed kinematic relations, Lagrange derivation, and explicit matrix forms are provided in Sections S1 and S2 of the electronic supplementary materials (ESM).

In terms of aerodynamic modeling, this study employs the Grossman quasisteady aerodynamic theory (Ye, 2016). This theory is established based on the assumptions of thin airfoils, small disturbances, and two-dimensional inviscid flow. Within this framework, both the main wing and the pre-wing can be treated as flat-plate airfoils, with their aerodynamic forces represented by a continuous distribution of bound vortices. The detailed derivation based on the vortex distribution, Kutta–Joukowski theorem, boundary condition, and aerodynamic moment integration is provided in Section S1 of the ESM.

It should be noted that the actual pre–main wing configuration involves viscous and unsteady flow phenomena, including wake interference, vortex evolution, and separation suppression, which cannot be explicitly resolved by the quasisteady inviscid model. However, the purpose of this study is to evaluate the first-order influence of pre-wing parameters on the flutter boundary rather than to reproduce detailed flow structures. Since classical linear flutter is mainly governed by aerodynamic stiffness, aerodynamic damping, and the phase relationship between aerodynamic forces and structural motion, the present low-order model is suitable for comparative flutter analysis. To compensate for its limitations, CFD-derived stability derivatives are introduced to calibrate the aerodynamic effects induced by the pre-wing.

3 Flutter characterization of the 2D pre–main wing combined configuration

3.1 System eigenvalue matrix

For the 2D pre-main wing combined configuration, the plunging displacement, pitching angle, and pre-wing equivalent deflection are selected as generalized coordinates. In the eigenvalue-based flutter analysis, these coordinates are assumed to undergo harmonic motion with the same modal frequency:

$$h = h_0 \mathrm{e}^{\mathrm{i}\omega t}, \quad \alpha = \alpha_0 \mathrm{e}^{\mathrm{i}\omega t}, \quad \varepsilon = \varepsilon_0 \mathrm{e}^{\mathrm{i}\omega t} \tag{3}$$

where h_0, α_0 and ε_0 are complex amplitudes. Substituting these expressions into the aeroelastic equations yields a velocity-dependent state-space system. The flutter boundary is determined by tracking the real parts of the eigenvalues as the flow velocity increases. When $\mathrm{Re}(\lambda) = 0$, the corresponding velocity is defined as the critical flutter speed, and the flutter frequency is obtained from $f = \mathrm{Im}(\lambda)/(2\pi)$. The detailed state-space formulation and eigenvalue expression are provided in Section S2 of the ESM.

3.2 Flutter characteristics: combined vs. conventional wing

3.2.1 Conventional wing flutter analysis

A conventional 2-DOF wing section is first analyzed to determine the baseline flutter boundary. The aerodynamic derivatives are obtained from simulation analysis under *Ma* = 0.15 and Reynolds number *Re* = 3.94×10^6, and the structural parameters are taken from Platanitis and Strganac (2004). The complete computational parameters are listed in Table S1 of the electronic supplementary materials.

For the conventional 2-DOF wing section, the plunge and pitch motions are selected as the generalized coordinates. Based on the aeroelastic model described above, the corresponding generalized mass, damping, and stiffness matrices are assembled to form the velocity-dependent state-space system. The explicit matrix expressions are listed in Section S2 of the ESM to avoid unnecessary repetition in the main text. By solving the eigenvalue problem of the state-space matrix at different flow velocities, the variation of the real parts of the eigenvalues is obtained.

As shown in Fig. 5, the eigenvalues' real parts are negative at zero velocity, indicating stability. The natural frequencies are 1.4354 Hz for plunge and 2.8932 Hz for pitch. The critical flutter speed is 14.2553 m/s with a flutter frequency of 1.4947 Hz. The plunge eigenvalue remains negative at all velocities, so it does not influence flutter onset. Overall, the flutter speed and frequency of the 2-DOF system are 14.2553 m/s and 1.4947 Hz, respectively. The natural frequency decreases by 48.34% before flutter.

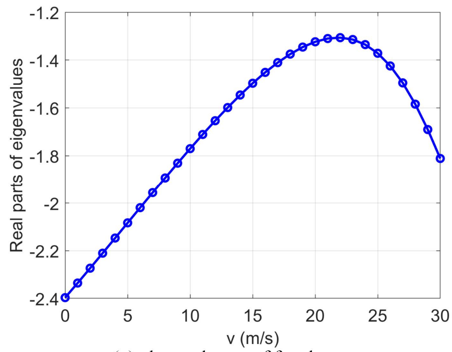

(a) plunge degree of freedom

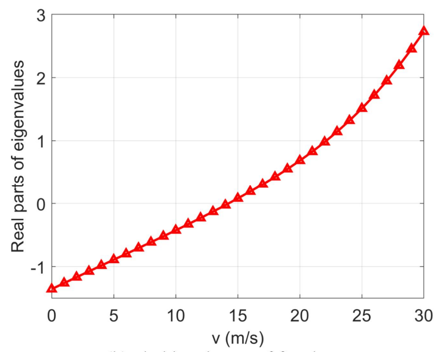

(b) pitching degree of freedom

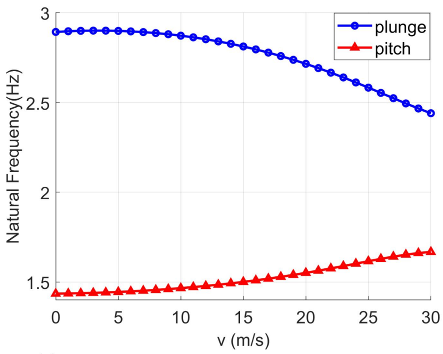

(c)

Fig. 5 Velocity vs. real parts of eigenvalues for a 2-DOF system: (a) plunge degree of freedom; (b) pitching degree of freedom; (c) velocity vs. natural frequency

3.2.2 Flutter analysis of the combined configuration

For the 3-DOF combined configuration, the aerodynamic derivatives are updated using CFD results to account for the influence of the pre-wing. The calculations are conducted at *Ma* = 0.15 and a Reynolds number *Re* = 3.94×10^{6}. The representative case uses a main-wing chord of 1 m and a pre-wing with *a* = 20 mm, *d* = 10 mm, located 20 mm ahead of and 20 mm above the main-wing leading edge. The updated parameters are summarized in Table S2 of the electronic supplementary materials. The corresponding mass, damping, and stiffness matrices are assembled using the formulation described in Section 2.2. Their explicit forms are provided in Section S2 of the electronic supplementary materials. The velocity-dependent state-space matrix is then constructed, and its eigenvalues are solved over the prescribed velocity range.

The variation in the real parts of the eigenvalues with flow velocity is shown in Fig. 6. The eigenvalue's real part becomes zero at 30.7578 m/s, indicating flutter onset at 3.4181 Hz. The pitch remains stable. For pre-wing deflection, the natural frequency is 1.4055 Hz, which is negative at low velocities but reaches zero at 20.4687 m/s, signaling instability and flutter at 1.4952 Hz. The critical flutter speed is 20.4687 m/s with a frequency of 1.4952 Hz.

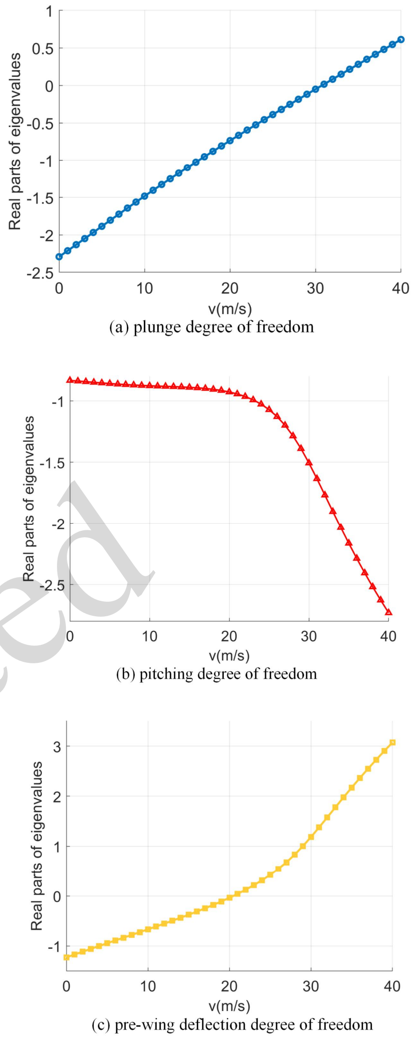

(a) plunge degree of freedom

(b) pitching degree of freedom

(c) pre-wing deflection degree of freedom

Fig. 6 Velocity vs. eigenvalue real part relationship for 3-DOF systems: (a) plunge degree of freedom; (b) pitch degree of freedom; (c) pre-wing deflection degree of freedom

According to the calculation results in Fig. 7, the natural frequency of the critical mode increases by 1.76% before flutter onset. After introducing the pre-wing, the flutter boundary is governed by the pre-wing equivalent deflection mode rather than the plunge mode, indicating that the pre-wing changes the aeroelastic characteristics of the system.

Table 2 compares the key aerodynamic derivatives and critical flutter speeds of the baseline and combined configurations. With the pre-wing, the lift coefficient decreases by 33.38%, while the pitching-moment derivative changes only slightly. The critical flutter speed increases from 14.2553 m/s to 20.4687 m/s, corresponding to an increase of

43.59%.

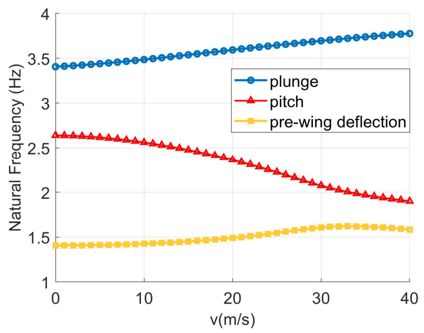

Fig. 7 Velocity versus natural frequency for 3-DOF systems

Table 2 Measured data of the experiments in five states

Parameters	Baseline value	Add the pre-wing	Change
$C_{l\alpha}$ (/rad)	1.5	0.9992	33.38%
$C_{m\alpha}$ (/rad)	0	-0.0014	0.14%
Critical speed of flutter(m/s)	14.2553	20.4687	43.59%

4 Study of the correlation between design parameters and flutter suppression characteristics

4.1 Relative location effects

The vertical and chordwise distances determine the relative position between the pre-wing and the main wing. Using these parameters, positions can be classified into three categories: directly in front of the main wing, above and ahead of the main wing, and below and ahead of the main wing (Fig. 8).

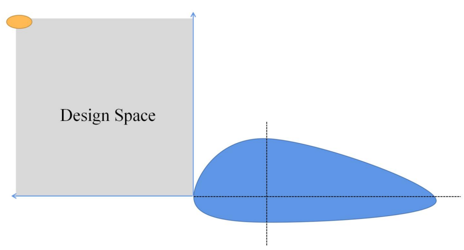

Fig. 8 Schematic of the influence of relative positions

Based on previous findings (Mi and Bai, 2022), an excessively small spacing between the pre-wing and the main wing may cause flow blockage, whereas an excessively large spacing weakens the wake interaction before it reaches the main wing. Therefore, this study focuses on a physically constrained design region where the pre-wing can still produce effective flow control. The results should be interpreted as locally effective solutions, and superior configurations may still exist outside the investigated design space.

4.1.1 Conventional wing flutter analysis

The pre-wing is first placed directly in front of the main wing, with the vertical offset fixed at 0 mm. The pre-wing size is kept constant at a = 10 mm and d = 5 mm, while the chordwise distance is varied from p_1/c =0.02 to 0.12. The complete stability derivatives and flutter results are listed in Table S3 of the electronic supplementary materials.

As shown in Fig. 9, the critical flutter speed is higher than that of the baseline wing at all sampled positions. The maximum improvement occurs at p_1/c =0.02, where the critical flutter speed reaches 26.3274 m/s, corresponding to an increase of 84.68%. When the distance increases to p_1/c =0.04, the improvement decreases to 29.13%, after which the flutter speed gradually increases again. This indicates that the chordwise position of the pre-wing strongly affects the flutter boundary.

4.1.2 Conventional wing flutter analysis

In this subsection, the pre-wing is arranged above and ahead of the main wing along a diagonal direction, while its size remains unchanged at a=10 mm and d=5 mm. The diagonal position is denoted by $(p_1/c, p_2/c)$. The sampled positions range from (0.02, 0.02) to (0.12, 0.12), and the complete stability derivatives and flutter results are provided in Table S4.

As shown in Fig. 9, the critical flutter speed first decreases and then gradually increases with increasing diagonal distance. The lowest value appears near $(p_1/c, p_2/c)$ =(0.03, 0.03), where the critical speed is 17.9527 m/s, which remains higher than that of the baseline wing. As the diagonal distance further increases, the critical speed recovers and reaches 21.1650 m/s at $(p_1/c, p_2/c)$ =(0.12, 0.12), corresponding to an increase of 48.47% compared with the baseline wing.

Compared with the direct front of the main wing arrangement, the diagonal arrangement provides a more stable improvement in the critical flutter speed at larger distances. Based on the identified turning point, the position near $(p_1/c, p_2/c)$ =(0.04,0.04) shows a more favorable flutter-speed increase.

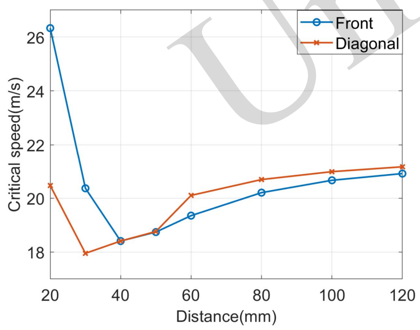

Fig. 9 Flutter critical velocity vs. pre-wing position

4.2 Relative size effects

The long and short axes indicate the relative size of the pre-wing. In size-effect studies, the pre-wing is consistently positioned directly in front of the main wing, with the distance from the leading edge starting at 20 mm. This distance is gradually increased to evaluate the critical flutter speed for each configuration. The analysis is conducted under three design conditions: (1) a = 10 mm, d = 5 mm (baseline configuration). (2) a = 20 mm, d = 5 mm. (3) a = 20 mm, d = 10 mm.

The first condition, previously calculated, serves as a reference for comparison. The results of the flutter characteristics are summarized in Fig. 10.

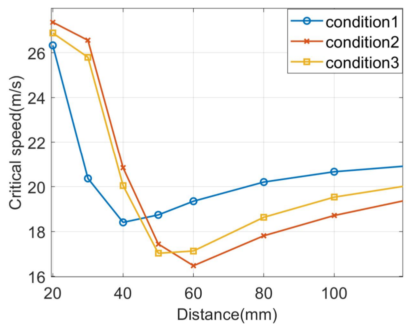

Fig. 10 Comparison of the critical flutter speed for three cases

For spacings below 50 mm, the shorter long axis provides better flutter suppression, whereas the longer long axis becomes more effective at larger spacings. When the long axis is fixed, increasing the short axis mainly changes the suppression magnitude rather than the overall trend; its effect becomes more pronounced as the spacing increases.

The effective design parameters are as shown in Fig. 11. For distances less than 40 mm, the pre-wing is positioned directly in front of the main wing, with a long axis length of a = 20 mm, short axis length of d = 5 mm, and an aspect ratio of a/d = 4. For distances beyond 40 mm, the pre-wing is arranged along the diagonal, with a = 10 mm, d = 5 mm, and a/d =2.

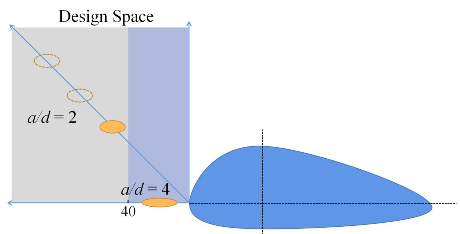

Fig. 11 Effective design parameters of the pre-wing

5 Conclusions

This study investigates the flutter characteristics of a two-dimensional prepositive elliptical wing–main wing combined configuration using a reduced-order aeroelastic model and CFD-evaluated aerodynamic derivatives. The main conclusions are as follows:

1. By modifying the local flow field of the main wing, the pre-wing changes the aerodynamic properties, generalized system matrix, and critical flutter condition of the aeroelastic system.

2. The eigenvalue-based analysis shows that under the representative operating conditions, the critical flutter speed increases by approximately 43.59% after introducing the pre-wing, confirming its effectiveness in improving flutter characteristics.

3. Strong coupling exists between the effects of pre-wing size and position. For chordwise distances within 0.04*c* (where c is the main wing chord), the elliptical wing is positioned directly in front of the main wing with a/c = 0.02, d/c = 0.005, and a/d = 4; beyond 0.04*c*, the wing is arranged along the diagonal with a/c = 0.01, d/c = 0.005, and a/d = 2.

4. Limitations of this work mainly arise from the 2D inviscid thin-airfoil assumption, incomplete design-space exploration, and the absence of formal optimization. Although suitable for preliminary flutter analysis and trend studies, the present model neglects viscous effects and three-dimensional spanwise flow structures and cannot fully capture vortex evolution, wake deformation, or spanwise coupling induced by the pre-wing. Moreover, because the two-dimensional airfoil model represents an infinite-span wing, its accuracy is limited for finite-span pre-wing configurations. Future studies should employ three-dimensional aeroelastic models, high-fidelity CFD methods, and optimization algorithms to explore broader parameter ranges and further clarify the flutter suppression mechanism.

Acknowledgments

This work is supported by the National Natural Science Foundation of China (Grant No. 12202363), the Innovation Foundation for Doctor Dissertation of Northwestern Polytechnical University (06010-24GH01020101), and the Natural Science Foundation of Chongqing (Grant No. CSTB2023NSCQ-MSX0042).

Author contributions

Congyu ZHAO developed the methodology, established the aeroelastic model, performed the eigenvalue-based flutter analysis, analyzed the results, created the visualizations, and drafted the manuscript. Baigang MI conceptualized the prepositive elliptical wing–main wing combined configuration, supervised the research, and reviewed and edited the manuscript. Xuan BAI carried out the CFD calculations and provided the aerodynamic data for the aeroelastic analysis.

Conflict of interest

Congyu ZHAO, Baigang MI, Xuan BAI declare that they have no conflict of interest.

Declaration on the use of generative AI tools

During the preparation of this work, the authors used ChatGPT to improve language. After using this tool, the authors reviewed and edited the content as needed and take full responsibility for the content of the publication.

Data availability

The data that support the findings of this study are available from the corresponding author upon reasonable request.

References

Guo Q, Li X, Zhou Z, Ma D, Wang Y, 2025. Neural network-based aeroelastic system identification for predicting flutter of high flexibility wings. *Scientific Reports*, 15(1):623. https://doi.org/10.1038/s41598-024-82573-7

Najmi J, Khan HA, Javaid SS, Hameed A, Siddiqui F, 2024. Aeroelastic tailoring for aerospace applications. *Heliyon*, 10(2):e24151. https://doi.org/10.1016/j.heliyon.2024.e24151

Borglund D, Kuttenkeuler J, 2002. Active wing flutter suppression using a trailing edge flap. *Journal of Fluids and Structures*, 16(3):271–294. https://doi.org/10.1006/jfls.2001.0426

Fernandez-Escudero C, Prothin S, Laurendeau E, Ross A, Michon G, 2023. Nonlinear flap for passive flutter control of bidimensional wing. *Journal of Vibration and Control*, *30*(23-24):5476-5485. https://doi.org/10.1177/10775463231223778

Nissim E, 1971. Flutter suppression using active controls based on the concepts of aerodynamic energy. Technical Report No. L-7525, NASA Langley Research Center, Hampton, VA, United States.

Strganac TW, Ko J, Thompson DE, Kurdila AJ, 2000. Identification and control of limit cycle oscillations in aeroelastic systems. *Journal of Guidance, Control, and Dynamics*, 23(6): 1127-1133. https://doi.org/10.2514/2.4664

Patil MJ, Hodges DH, 2002. Output feedback control of the nonlinear aeroelastic response of a slender wing. *Journal of Guidance, Control, and Dynamics*, 25(2):302-308. https://doi.org/10.2514/2.4882

Behal A, Marzocca P, Rao VM, et al., 2006. Nonlinear adaptive control of an aeroelastic two-dimensional lifting surface. *Journal of Guidance, Control, and Dynamics*, 29(2):382-390. https://doi.org/10.2514/1.14011

Theis J, Pfifer H, Seiler P, 2020. Robust modal damping control for active flutter suppression. *Journal of Guidance, Control, and Dynamics*, 43(6):1056-1068.

https://doi.org/10.2514/1.G004846
Ribeiro FA, Geronel RS, De Marqui Junior C, Bueno DD, 2025. An efficient approach to design robust controllers for active flutter suppression. *Journal of Sound and Vibration*, 617:119296. https://doi.org/10.1016/j.jsv.2025.119296
Chen Z, Shi ZW, Chen SN, Liao XQ, Mei Y, 2023. Active flutter suppression on a flexible wing via leading-edge blowing and circulation control. *Physics of Fluids*, 35(9):097124. https://doi.org/10.1063/5.0162013
Chen CL, Chang CW, Yau HT, 2012. Terminal sliding mode control for aeroelastic systems. *Nonlinear Dynamics*, 70(3):2015-2026. https://doi.org/10.1007/s11071-012-0593-x
Mu X, Huang R, Zou Q, Hu H, 2022. Machine learning-based active flutter suppression for a flexible flying-wing aircraft. *Journal of Sound and Vibration*, 529:116916. https://doi.org/10.1016/j.jsv.2022.116916
Sun Z, Jin C, 2023. Advances in nonlinear dynamics for delayed systems. *Journal of Dynamics and Control,* 21(8):6-18 (in Chinese). 10.6052/1672-6553-2023-024
Sinou JJ, 2022. Flutter instability and active aeroelastic control with time delay for a two-dimensional airfoil. *European Journal of Mechanics - A/Solids,* 92:104465. https://doi.org/10.1016/j.euromechsol.2021.104465
Wu Y, Dai Y, Yang C, 2022. Time-delayed active control of stall flutter for an airfoil via camber morphing. *AIAA Journal*, 60(10):5723-5734. https://doi.org/10.2514/1.J061947
Ouyang Y, Gu Y, Ku X, Yang Z, 2021. Active flutter suppression of wing with morphing flap. *Aerospace Science and Technology*, 110:106457. https://doi.org/10.1016/j.ast.2020.106457
Gu Y, Yang Z, 2006. Aerodynamic response analysis of an airfoil with hysteresis nonlinearity. *Mechanical Science and Technology for Aerospace Engineering*, 25(8):900-904 (in Chinese). 10.3321/j.issn:1003-8728.2006.08.005
Li D, Xiang J, 2007. Analysis of flutter characteristics of bipartite wings with hysteretic nonlinearities. *Acta Aeronautica et Astronautica Sinica*, 28(3):600-604 (in Chinese). 10.3321/j.issn:1000-6893.2007.03.019
Ouyang S, Gu Y, 2010. Simulation study of active nonlinear flutter suppression based on unsteady vortex aerodynamic theory. *Mechanical Science and Technology for Aerospace Engineering*, 29(8):1060-1064 (in Chinese). 10.13433/j.cnki.1003-8728.2010.08.015
Mi B, Bai X, 2022. New flow control techniques with prepositioned stationary or vibrating elliptical wing at low speed and high angle of attack. *Journal of Aerospace Engineering*, 35(5):04022064. https://doi.org/10.1061/(ASCE)AS.1943-5525.0001433
Bai X, Zhan H, Mi B, 2025. Unsteady aerodynamic force modeling method for prepositive elliptical wing-main wing composite flow control configurations at high angles of attack. *Physics of Fluids*, 37(6):065140. https://doi.org/10.1063/5.0272561
Ye ZY, 2016. Fundamentals of Fluid-Structure Coupling and Its Applications, 2nd Edition. Harbin Institute of Technology Press, Harbin, China, p.63-66 (in Chinese).
Platanitis G, Strganac TW, 2004. Control of a nonlinear wing section using leading and trailing-edge surfaces. *Journal of Guidance, Control, and Dynamics*, 27(1):52 – 58. https://doi.org/10.2514/1.9284

Electronic supplementary materials

Section S1-S3, Table S1-S4

中文概要

题　目：二维前置椭圆翼–主翼复合构型的颤振特性

作　者：赵聪予[1,2]，米百刚[1]，白璇[1,2]
机　构：[1]西北工业大学，航空学院，中国西安，710072；[2]飞行器基础布局全国重点实验室，中国西安，710072

目　的：颤振是飞行器结构与气动力耦合作用下产生的自激振动失稳问题，严重威胁飞行安全。传统颤振抑制方法通常依赖结构参数调整、控制面作动或主动控制系统，可能增加系统复杂性或改变原有气动特性。本文提出一种二维前置椭圆翼–主翼复合构型，研究前置椭圆翼对主翼颤振特性的影响，旨在探索一种被动颤振边界改善方法。

创新点：1. 提出在主翼前方布置椭圆翼的颤振抑制方法，通过形成前置椭圆翼–主翼复合构型调节主翼局部流场和气动能量输入；2. 基于结构动力学建立二维复合构型的低阶气动弹性模型，并结合 CFD 计算的气动导数，利用特征值法计算临界颤振速度；3. 定量表明前置椭圆翼可使代表性构型的临界颤振速度提高 43.59%；4. 分析前置翼位置、长短轴尺寸及长短轴比对颤振特性的耦合影响，给出有效设计参数范围，为后续组合构型气动弹性优化提供参考。

方　法：1. 在小扰动、二维薄翼和准定常气动力假设下，建立前置椭圆翼–主翼复合构型的低阶气动弹性模型，将前置翼影响等效为主翼气动导数和广义气动坐标的变化；2. 通过 CFD 计算获得组合构型的气动导数，并将其引入气动弹性方程，采用特征值法求解不同构型下的临界颤振速度和颤振频率；3. 改变前置翼相对位置、长轴、短轴和长短轴比，比较不同参数组合对临界颤振速度的影响，确定有效

的构型参数范围。

结　论： 1. 前置椭圆翼能够改变主翼局部流场和气动特性，进而影响气动弹性系统的广义系统矩阵和临界颤振条件；2. 代表性计算结果表明，引入前置翼后，组合构型的临界颤振速度由 14.2553 m/s 提高到 20.4687 m/s，提高幅度约为 43.59%，说明前置翼对改善颤振特性具有明显作用；3. 前置翼位置和尺寸对颤振特性具有耦合影响。当弦向距离小于或等于 0.04c 时，推荐采用主翼正前方布置，参数为 a/c = 0.02、d/c = 0.005、a/d = 4；当距离大于 0.04c 时，推荐采用前上方斜向布置，参数为 a/c = 0.01、d/c = 0.005、a/d = 2。

关键词： 气动弹性；特征值法；被动流动控制；数值模拟